



CHORUS

This is the accepted manuscript made available via CHORUS. The article has been published as:

High-intensity-beam study of $^{17}\text{O}(p,\gamma)^{18}\text{F}$ and thermonuclear reaction rates for $^{17}\text{O}+p$

M. Q. Buckner, C. Iliadis, K. J. Kelly, L. N. Downen, A. E. Champagne, J. M. Cesaratto, C. Howard, and R. Longland

Phys. Rev. C **91**, 015812 — Published 30 January 2015

DOI: [10.1103/PhysRevC.91.015812](https://doi.org/10.1103/PhysRevC.91.015812)

High-intensity beam study of $^{17}\text{O}(p,\gamma)^{18}\text{F}$ and thermonuclear reaction rates for $^{17}\text{O}+p$

M. Q. Buckner,^{1,2} C. Iliadis,^{1,2} K. J. Kelly,^{1,2} L. N. Downen,^{1,2} A. E. Champagne,^{1,2} J. M. Cesaratto,^{1,2} C. Howard,^{1,2} and R. Longland^{3,2}

¹*Department of Physics and Astronomy, University of North Carolina,*

Chapel Hill, North Carolina, 27599-3255, USA

²*Triangle Universities Nuclear Laboratory,*

Durham, North Carolina 27708-0308, USA

³*Department of Physics and Astronomy, North Carolina State University,*

Raleigh, North Carolina, 27708-0308, USA

(Dated: January 5, 2015)

Abstract

Hydrogen burning of the oxygen isotopes takes place in low-mass stars, AGB stars, and classical novae. Observations of oxygen elemental and isotopic abundances in stellar spectra or in presolar grains provide strong constraints for stellar models if reliable thermonuclear reaction rates for hydrogen burning of oxygen are available. We present the results of a new measurement of the $^{17}\text{O}(p,\gamma)^{18}\text{F}$ reaction in the laboratory bombarding energy range of 170–530 keV. The measurement is performed with significantly higher beam intensities ($I_{max} \approx 2$ mA) compared to previous work and by employing a sophisticated γ -ray coincidence spectrometer. We measured the cross section at much lower energies than previous in-beam experiments. We also apply a novel data analysis technique that is based on the decomposition of different contributions to the measured pulse-height spectrum. Our measured strengths of the low energy resonances amount to $\omega\gamma_{pres}(193 \text{ keV}) = (1.86 \pm 0.13) \times 10^{-6}$ eV and $\omega\gamma_{pres}(518 \text{ keV}) = (13.70 \pm 0.96) \times 10^{-3}$ eV. For the direct capture S-factor at zero energy, we find a value of $S_{DC}^{pres}(0) = 4.82 \pm 0.41$ keVb. We also present new thermonuclear rates for the $^{17}\text{O}+p$ reactions, taking into account all consistent results from previous measurements.

I. INTRODUCTION

Hydrogen burning of the oxygen isotopes takes place in a variety of sites, including low-mass stars during hydrogen core and shell burning [1], AGB stars during hydrogen shell burning [2], intermediate-mass AGB stars during hot-bottom burning [3], and both CO and ONe classical novae during explosive hydrogen burning [4]. Observations of oxygen elemental and isotopic abundances in stellar spectra [5] or in presolar grains [6] can provide strong constraints for stellar model simulations if reliable thermonuclear reaction rates for the hydrogen burning of oxygen are available over a wide region of stellar temperatures. Rates for the $^{16}\text{O}(p,\gamma)^{17}\text{F}$ reaction, with an uncertainty of less than 7%, were derived by Ref. [7] and the most recent $^{18}\text{O}+p$ reaction rates can be found in Refs. [8, 9]. Here, we present new thermonuclear rates for the $^{17}\text{O}+p$ reactions.

The ^{18}F level scheme is shown in Fig. 1. The first modern $^{17}\text{O}+p$ thermonuclear reaction rates, based on a comprehensive set of directly measured yield data and including a detailed understanding of the ^{18}F level structure, were published by Rolfs & Rodney [10] and by Kieser et al. [11]. A decade later, Landre et al. [12] obtained valuable information by studying the ^{18}F levels near the proton threshold via the $^{17}\text{O}(^3\text{He},d)^{18}\text{F}$ transfer reaction. Subsequently, Blackmon et al. [13] directly measured a low-energy resonance at a bombarding energy near 60 keV in the $^{17}\text{O}(p,\alpha)^{14}\text{N}$ reaction. Recent years have seen a flurry of activity. Fox et al. [14, 15] discovered a new resonance in the $^{17}\text{O}(p,\gamma)^{18}\text{F}$ reaction at a bombarding energy of 193 keV. This measurement was confirmed by Chafa et al. [16, 17], who also discovered the corresponding resonance in the (p,α) reaction channel. Subsequent work, using different experimental techniques, verified their results [18, 19]. Fox et al. [15] first pointed out that the non-resonant (direct capture) process dominates the total thermonuclear $^{17}\text{O}(p,\gamma)^{18}\text{F}$ rates over wide temperature regions. This expectation was verified by Newton et al. [20] by directly measuring the total astrophysical S-factor in the bombarding energy range of 275 – 500 keV. Their results were in contradiction, both in magnitude and energy-dependence, with the earlier low-energy S-factor reported by Rolfs [21]. Kontos et al. [22] measured the $^{17}\text{O}(p,\gamma)^{18}\text{F}$ reaction at higher energies, in the range of 345 – 1700 keV, and extracted the low-energy S-factor from an R-matrix analysis of the data. Additional low-energy S-factor data for the $^{17}\text{O}(p,\gamma)^{18}\text{F}$ reaction were recently obtained in inverse kinematics by Hager et al. [23], at energies of 265 – 530 keV, and by the LUNA

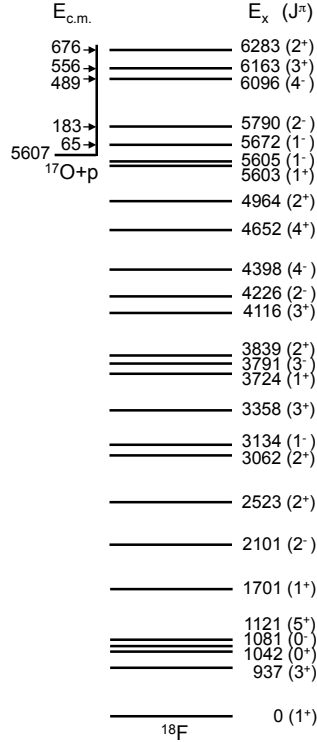


FIG. 1. Energy level diagram of ^{18}F . Most excitation energies and J^π values are from Ref. [51]; we adopted improved values for some levels (see text). The proton separation energy (5607 keV) is from Ref. [52]. Only levels relevant for the present work are displayed. All energies are in units of keV.

(Laboratory Underground for Nuclear Astrophysics) collaboration [24, 25], at bombarding energies between 171 keV and 392 keV.

Because of the astrophysical importance of the $^{17}\text{O}(p,\gamma)^{18}\text{F}$ reaction rate, we performed a new measurement at bombarding energies between 170 keV and 530 keV. A new measurement is justified for a number of reasons. The LUNA experiment was performed in the underground Gran Sasso National Laboratory, using proton beam intensities of $\approx 200 \mu\text{A}$ and measuring both the prompt γ -ray emission and the beam-induced activity using a single HPGe detector. Their prompt γ -ray data reach a minimum bombarding energy of 212 keV. Below this energy, only two data points were measured (at 171 keV and 176 keV), using the activation method, but they do not agree within $1\text{-}\sigma$ uncertainties. Furthermore, the low-energy S-factor obtained by Kontos et al. [22] is systematically higher than the LUNA results by $\approx 13\%$. Therefore, an independent measurement is warranted.

In the present work, we apply a technique that has not been employed in previous $^{17}\text{O}(p,\gamma)^{18}\text{F}$ reaction studies. It must be kept in mind that the sensitivity in a nuclear counting experiment is *directly* proportional to the signal count rate, and therefore, increasing the proton beam current is of utmost importance. Our maximum beam current amounts to ≈ 2 mA, which represents an order of magnitude improvement over Ref. [25]. Furthermore, the sensitivity is approximately inversely proportional to the *square root* of the background count rate. Thus we perform the measurements using a coincidence $\gamma\gamma$ -spectrometer, which allows not only for a significant reduction in background, but also provides valuable experimental information for the interpretation of the ^{18}F decay scheme at each measured energy.

The experimental apparatus is described in Sec. II. The data analysis and our resonance strengths and S-factors for $^{17}\text{O}(p,\gamma)^{18}\text{F}$ are presented in Sec. III. New thermonuclear reaction rates for $^{17}\text{O}(p,\gamma)^{18}\text{F}$ and $^{17}\text{O}(p,\alpha)^{14}\text{N}$ are derived in Sec. IV by taking all of the available experimental information into account. A summary and conclusions are given in Sec. V.

II. EQUIPMENT

A. Ion beam and targets

The experiment was carried out at the Laboratory for Experimental Nuclear Astrophysics (LENA), which is part of the Triangle Universities Nuclear Laboratory (TUNL). The LENA facility houses two accelerators. The JN Van de Graaff accelerator is capable of producing proton beams of up to $120\ \mu\text{A}$ on target in the energy range below $E_{lab} = 1$ MeV. The bombarding energy was calibrated with well-known resonances in $^{18}\text{O}(p,\gamma)^{19}\text{F}$ and $^{27}\text{Al}(p,\gamma)^{28}\text{Si}$ [27, 28]. The JN accelerator, which typically achieves a beam resolution of ≈ 2 keV, was used for collecting some of the low-energy yield data (≥ 250 keV), and for measuring excitation functions to monitor the target thickness and stability during the experiment. The second accelerator consists of a high-current, low-energy electron cyclotron resonance ion source (ECRIS). The LENA ECRIS produces a maximum beam current of ≈ 2.0 mA on target, with an average beam current of ≈ 1.2 mA over extended periods of time. It was used to collect data at bombarding energies below 200 keV. Detailed information regarding the facility can be found in Ref. [26].

During the course of the experiment, the proton beam from either accelerator entered the target chamber through a liquid-nitrogen cooled copper tube. An electrode was mounted at the end of this tube and was biased to -300 V in order to suppress the emission of secondary electrons from the target and the beam collimator. The target and chamber formed a Faraday cup for charge integration. The beam was focused and rastered into a circular profile of ≈ 12 mm diameter on target. The target was directly water cooled using deionized water.

Targets of ^{17}O were prepared by anodizing 0.5 mm thick tantalum backings in ^{17}O -enriched water. According to the supplier, the water composition (in atom %) was 87.7 (^{17}O), 11.6 (^{16}O), and 0.7 (^{18}O). Such targets were found [29] to have a well-defined stoichiometry (Ta_2O_5) with a target thickness that is precisely determined by the anodizing voltage. Prior to target fabrication, the surfaces of the tantalum backings were etched, and the backings were outgassed in vacuum by resistive heating to reduce impurities that cause beam-induced background radiation. The thicknesses of our ^{17}O targets were measured using well-known resonances in $^{17}\text{O}(p,\gamma)^{18}\text{F}$ ($E_r^{lab} = 518$ keV [15]) and $^{18}\text{O}(p,\gamma)^{19}\text{F}$ ($E_r^{lab} = 151$ keV [27]), and were found to be 11 keV and 16 keV, respectively. The small thickness simplified the extraction of the effective interaction energy and S-factor from the measured yield (see Sec. III). Yield curves of the 518 keV resonance (see Fig. 2) were measured frequently to quantify the target degradation. The targets withstood beam charge accumulations up to 55 C at a beam intensity of ≈ 2.0 mA without any degradation in the maximum height of the yield curves. However, the width of the yield curves (i.e., the target thickness) reduced noticeably because of target sputtering (at a rate of $\approx 0.07 - 0.22$ keV/C, depending on the target and the beam intensity). Targets were discarded when the thickness degraded by more than 25%, which typically occurred at charge accumulations of ≈ 30 C. This modest effect was easily corrected for in the extraction of the total low-energy S-factor from the measured yield.

B. Spectrometer

At low bombarding energies, the $^{17}\text{O}(p,\gamma)^{18}\text{F}$ reaction gives rise to the emission of multiple, coincident γ -rays. Therefore, the simultaneous detection of two or more photons allows for a significant reduction in environmental background [30]. The detection setup is shown in

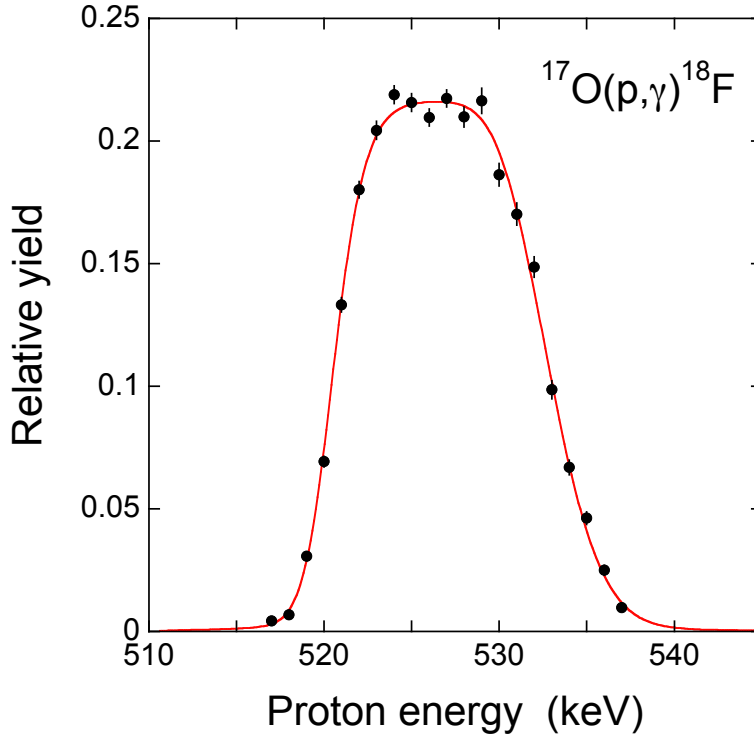


FIG. 2. (Color online) Excitation function of the primary $R \rightarrow 1121$ keV transition for the well-known $^{17}\text{O}(p,\gamma)^{18}\text{F}$ resonance at $E_r^{\text{lab}} = 518$ keV. The uncertainties derive from counting statistics only. The red line represents a fit, using a Markov Chain Monte Carlo method, to extract the maximum yield, target thickness, and area under the yield curve.

Fig. 3. The LENA $\gamma\gamma$ -coincidence spectrometer consists of an 135% HPGe detector, which is oriented at zero degrees with respect to the beam axis and is surrounded by a 16-segment NaI(Tl) annulus. The distance between the HPGe detector and the target midpoint was 1.1 cm. Since the HPGe detector covered a large solid angle, it integrated over a significant part of the angular correlation function for anisotropic photon emission patterns. The NaI(Tl) annulus provides nearly 4π coverage and thus is insensitive to angular correlation effects. Plastic scintillator paddles of 5 cm thickness (not shown in the figure) covered the two counters on five sides and suppressed cosmic-ray muon events. The HPGe and NaI(Tl) counters were energy calibrated using radioactive sources (^{22}Na , ^{56}Co) and well-known resonances in $^{14}\text{N}(p,\gamma)^{15}\text{O}$ ($E_r^{\text{lab}} = 278$ keV [31]) and $^{18}\text{O}(p,\gamma)^{19}\text{F}$ ($E_r^{\text{lab}} = 151$ keV [27]). Further information concerning the detection system can be found in Ref. [32].

Raw timing and energy signals were processed using standard NIM and VME modules.

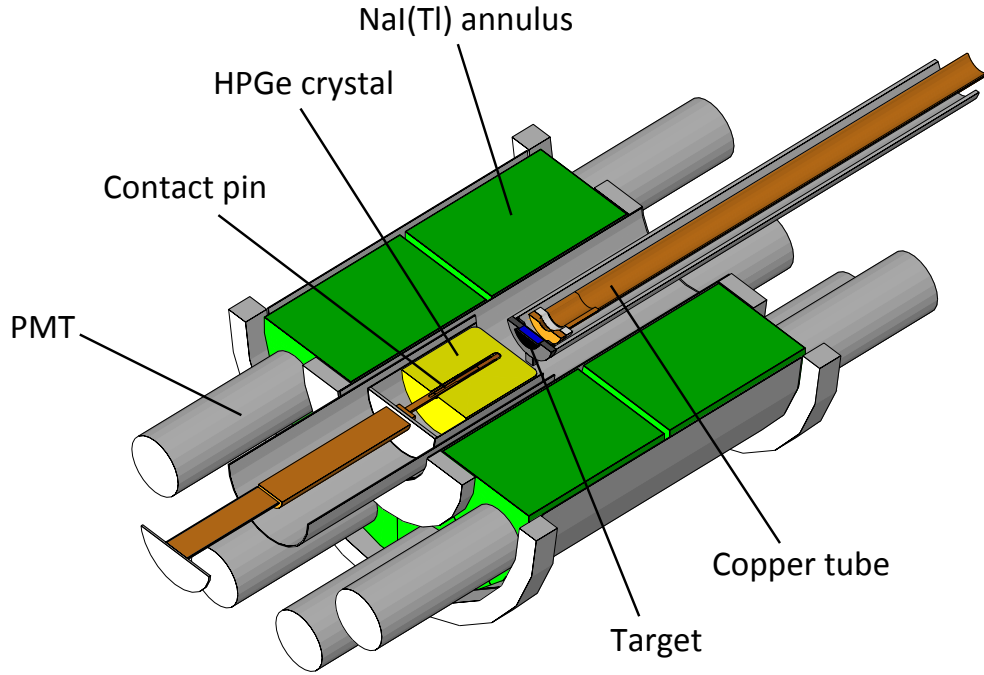


FIG. 3. (Color online) Coincidence spectrometer employed in the present work. The HPGe crystal (yellow) is located in close geometry to the target. Both the target and the HPGe detector are surrounded by a 16-segment NaI(Tl) annulus (green). The 5-sided plastic scintillators used to reject cosmic ray muons are not shown.

The HPGe signals served as the master trigger for the electronics. All events were sorted off-line using the acquisition software JAM [33] and all coincidence energy and timing gates were set in software. The HPGe-NaI(Tl) coincidence timing gate had to be set sufficiently wide (≈ 500 ns) because of the long mean lifetime of the $E_x = 1121$ keV level ($\tau_m = 234 \pm 10$ ns [34]) in ^{18}F . In the two-dimensional NaI(Tl) versus HPGe energy spectrum, a trapezoidal gate with the condition

$$3.5 \text{ MeV} \leq E_{\text{HPGe}} + E_{\text{NaI(Tl)}} \leq 9.0 \text{ MeV} \quad (1)$$

was applied. The low-energy threshold reduces the environmental background (^{40}K , ^{208}Tl , etc.) by about two orders of magnitude, while the high-energy threshold excludes events with a total energy somewhat exceeding the Q-value of $^{17}\text{O}(p,\gamma)^{18}\text{F}$ ($Q = 5.6$ MeV) plus the center-of-mass kinetic energy. Events above the high energy threshold are most likely caused by cosmic-ray muons and neutrons.

As will become apparent in Sec. III, it is important for the data analysis to accurately simulate the response of our $\gamma\gamma$ -coincidence spectrometer. The simulations were performed with the `Geant4` package, version 9.6 [35, 36]. The internal geometry of our HPGe detector is well known since it was previously measured [37] using computed tomography (CT). The dimensions of our spectrometer, including the annulus, are listed in Tab. 1 of Ref. [38]. The geometry was incorporated into the `Geant4` model of our setup, including surrounding material that could give rise to additional photon scattering and the extended beam spot size. It was shown in Ref. [38] that this model accurately simulates absolute singles and coincidence efficiencies of the LENA detection system for the decay of ^{60}Co and for the $E_r^{\text{lab}} = 151$ keV resonance in $^{18}\text{O}(p,\gamma)^{19}\text{F}$. Further validation tests are discussed in Sec. III.

III. DATA ANALYSIS AND RESULTS

A. Strategy

The usual problem faced in a prompt γ -ray counting measurement with a weak signal is the following: in fortunate cases, a number of primary and secondary decays for the reaction of interest are observed in a pulse height spectrum. The total number of reactions that took place, which determines the cross section or the resonance strength, can then be estimated from the sum of efficiency and summing corrected net intensities of either all observed primary decays or of all observed ground state decays (see, e.g., Ref. [40]). Weak, unobserved primary transitions will necessarily remain unaccounted for and estimates of their contributions based on the measured data alone are frequently problematic. This is the strategy that was employed, for example, in the recent studies of Refs. [20, 25] that analyzed measured *singles* HPGe spectra. When the data are subject to coincidence requirements, such as in the present work, this procedure becomes cumbersome because the net intensities need to be corrected by factors that depend not only on the efficiencies of both the HPGe and NaI(Tl) counters, but also on the branching ratios of the primary decays and angular correlations (see Eq. 4.84 in Ref. [40]). However, the primary branching ratios are *a priori* unknown unless additional information, beyond the measured data, is available. These problems could only be partially addressed in Refs. [9, 39].

In the present work we discuss a novel method that does not require explicit estima-

tions of efficiencies or coincidence summing. These effects, and others, including angular correlations, photon absorption, and the finite beam spot size, are implicitly included in our **Geant4** simulations. Additionally, the method does not assume prior knowledge of the primary branching ratios. It only requires knowledge of the spectrometer geometry (Sec. II B) and the branching ratios of all *secondary* decays (i.e., transitions in a cascade that occur after the primary decay, except for the ground state transition). The secondary branchings are well known [34] in the ^{18}F excitation energy range of interest. Details regarding our method will be presented in a forthcoming publication. In brief, consider a measured pulse-height spectrum, which is given by the sum of distinct components (or templates): room background, beam-induced background, and the reaction of interest. The latter component also consists of several different templates, with any given template containing a single primary decay and all corresponding secondary decays. If the contributions of each template that make up the experimental singles or coincidence spectrum could be extracted, then it is straightforward to estimate the primary branching ratios together with the total number of $^{17}\text{O}(p,\gamma)^{18}\text{F}$ reactions that took place at a given bombarding energy. This method of analysis uses the information contained in every single bin of the pulse height spectrum, including primary and secondary peaks, Compton scattering events, and escape peaks. It should also improve the estimation of unobserved primary decays because they presumably leave their imprint on secondary transitions if the latter decays are observed.

More specifically, the analysis involves the following steps. First, a measured singles or coincidence spectrum is energy calibrated using well-known decays from radioactive sources and nuclear reactions (Sec. II B). Second, the templates are generated. A measured spectrum without beam provides the template for the environmental background. All other templates are simulated with **Geant4**. Beam-induced peaks from ^{11}B , ^{14}N , ^{18}O , and ^{19}F contaminants in the target are easily identified in the experimental spectrum. Thus beam-induced templates are simulated, using the known decay scheme, for each of these contaminants. Furthermore, for each potential primary decay from $^{17}\text{O}(p,\gamma)^{18}\text{F}$, a template is simulated assuming known branchings for all subsequent secondary decays. All simulated spectra are convolved with energy-dependent resolution functions, so that the widths of corresponding observed and simulated peaks agree. Typically, each template is generated with 2,500,000 simulated events to ensure sufficient statistics. Angular correlations for all primary decays are included in the simulations (see below). We assumed isotropic angular correlations for all secondary decays.

Third, where coincidence spectra are concerned, the room background and the simulated events are analyzed with the same coincidence timing and energy gates as the measured data obtained with beam on target.

For each template, i , we obtain

$$\frac{N_i^{data}}{A_i^{data}} = \frac{N_i^{sim}}{A_i^{sim}} \quad (2)$$

where N_i^{data} denotes the number of primary decays of component i (or the partial number of $^{17}\text{O}+p$ reactions) that gave rise to the experimental spectrum, N_i^{sim} is the total number of simulated primary decays of component i , A_i^{data} is the total area (above a given threshold) in the experimental spectrum that is solely caused by component i , and A_i^{sim} is the corresponding total area in the simulated spectrum of component i . The final step involves the numerical decomposition of the measured spectra, which provides the *fraction* of the total area in the measured spectrum that arises from component i , $F_i = A_i^{data}/A_{total}^{data}$, where A_{total}^{data} denotes the total area in the measured spectrum. Thus we find

$$N_i^{data} = \frac{N_i^{sim}}{A_i^{sim}} F_i A_{total}^{data} \quad (3)$$

With all quantities on the right-hand side either measured or simulated, the partial number of $^{17}\text{O}+p$ reactions, N_i^{data} (i.e., for each primary decay, i), can be determined. Summing over all components gives the total number of $^{17}\text{O}+p$ reactions, $N_R^{data} = \sum_i N_i^{data}$, and the ratio of partial and total number of $^{17}\text{O}+p$ reactions gives the primary branching ratio, $B_i^{pri} = N_i^{data}/N_R^{data}$. The total number of $^{17}\text{O}+p$ reactions determines the yield from which the cross section (for a non-resonant process) or the resonance strength (for a resonance) can be computed.

The estimation of the fraction each template contributes to the measured singles or coincidence spectrum is performed using a binned maximum likelihood fit using Poisson statistics that takes into account the finite Monte Carlo statistics of the simulated templates [41]. The method assumes that the experimental spectrum is given by a linear combination of several template spectra with fixed shapes. The input templates are allowed to vary, bin by bin, within their statistical uncertainty, leading to additional contributions to the overall likelihood. For many fit parameters (one per bin per template), the minimization can be performed semi-analytically since the event numbers in each bin are independent. The only formal fit parameters to be determined numerically are the template fractions. The

template statistics need to be at least comparable to the statistics in the measured spectrum, although higher template statistics lower the fit uncertainties. We used the implementation of this method in Root's [42] `TFractionFitter` class¹, which uses the MINUIT minimization routine.

B. Resonance at $E_r^{lab} = 518$ keV

We have tested our analysis procedure by measuring the well-known $E_r^{lab} = 518$ keV resonance in $^{17}\text{O}(p,\gamma)^{18}\text{F}$. The strength was determined previously in three independent experiments [15, 21, 22], and the previously measured values agree within uncertainties. The primary decays of this resonance proceed to seven ^{18}F levels. Primary branching ratios have been reported in Refs. [22, 34]. The resonance is sufficiently strong that corrections for a non-resonant process or tails of higher-lying broad resonances can safely be disregarded.

In the present work, we accumulated 0.020 C of charge at a bombarding energy of $E_r^{lab} = 525$ keV, on the top of the thick-target yield curve. The measured singles and coincidence spectra, obtained using the condition of Eq. (1), were sorted off-line. Several templates were prepared for each measured spectrum: one using the experimental room background, and seven $^{17}\text{O}+p$ templates simulated with `Geant4`, i.e., one for each observed primary decay assuming known branching ratios for the subsequent *secondary* decays. This resonance is formed by p-wave capture [43, 44] and thus the channel spin amounts to $j_s = 3$. Under these conditions, it is straightforward to calculate the expected angular correlations of the primary transitions (see, e.g., Ref. [40]) and these were incorporated into the simulations. The measured spectra were then analyzed above an energy threshold of 800 keV to optimize the convergence of the fit.

The scaling factor of each template fraction, F_i , estimated by the fraction fitter is used to estimate the partial number of reactions for each primary transition, according to Eq. (3). From these values, the primary branching ratios were derived. These are listed in Tab. I, both for the singles and the coincidence spectrum, along with literature values [22, 34]. It can be seen that our values derived from the singles and the coincidence spectrum are in overall agreement. This test is important because it implies that our simulations accurately reproduce the response of the NaI(Tl) annulus. Our obtained primary branchings are also

¹ See: <http://root.cern.ch/root/html/doc/TFractionFitter.html>.

in good agreement with the literature values.

From the total number of $^{17}\text{O}+p$ reactions, N_R^{data} , the resonance strength, $\omega\gamma$, is calculated assuming a thick-target yield, Y , since the target thickness (11 keV, see Sec. II) is much larger than the total resonance width (240 eV [11]):

$$Y = \frac{N_R^{data}}{N_p} = \frac{\lambda^2 \omega\gamma}{2 \epsilon} \quad (4)$$

where N_p denotes the number of incident protons, λ is the de Broglie wavelength, and ϵ denotes the effective stopping power [20]. All quantities refer to the center of mass system. Common uncertainties derive from the charge integration (3%), effective stopping power (4%), and the simulation of the HPGe and NaI(Tl) detection efficiencies using **Geant4** (5%). The statistical uncertainty determined by the fraction fitter amounts to 1.2%. Our measured resonance strengths are listed in Tab. II together with literature values. The results of the older measurement by Sens, Paper and Armbruster [43] are disregarded because they disagree with all other values. It can again be seen that the resonance strength values derived from our singles and coincidence spectra are in agreement. Our mean value is $\omega\gamma_{pres}(518 \text{ keV}) = (13.70 \pm 0.96) \times 10^{-3} \text{ eV}$. This result also agrees with the previously reported values. The weighted average of all measurements, except for Ref. [43], amounts to $\omega\gamma_{rec}(518 \text{ keV}) = (13.3 \pm 0.7) \times 10^{-3} \text{ eV}$ (Tab. II).

C. Resonance at $E_r^{lab} = 193 \text{ keV}$

This resonance was first observed by Fox et al. ($\omega\gamma = 1.2 \pm 0.2 \mu\text{eV}$ [14, 15]), and subsequently measured by Chafa et al. ($\omega\gamma = 2.2 \pm 0.4 \mu\text{eV}$ [17]) and Di Leva et al. ($\omega\gamma = 1.67 \pm 0.12 \mu\text{eV}$ [25]). Di Leva et al. observed several more primary transitions compared to Refs. [14, 15] and they attributed the higher sensitivity to the fact that their measurement was performed deep underground. However, their accumulated on-resonance charge amounted to 95 C, which has to be compared to a value of 4.1 C accumulated in Fox et al. [15]. Therefore, it is clear that a significant fraction of the sensitivity increase originates from the larger accumulated charge.

In the present work, we accumulated a charge of 14 C, with an average beam intensity of $\approx 1.1 \text{ mA}$ on target. The measurement was performed at a bombarding energy of $E_p^{lab} = 200 \text{ keV}$, on top of the thick-target yield curve. Compared to the data analysis for the much

TABLE I. Primary branching ratios of low-energy resonances in $^{17}\text{O}(p,\gamma)^{18}\text{F}$.

$E_r^{lab} = 518 \text{ keV}, E_r^{cm} = 489 \text{ keV} (J^\pi = 4^-)$				
Transition	Tilley [34] ^a	Kontos [22]	present (coin)	present (sing)
R→937	4.9(9)	4.2(5)	5.7(3)	5.7(4)
R→1121	55(3)	58.6(23)	58.1(12)	59.5(11)
R→2101	27(2)	25.1(11)	26.9(6)	24.5(5)
R→3791	1.4(3)	1.3(2)	1.26(13)	2.03(13)
R→4116	1.8(3)	1.8(3)	1.63(12)	1.90(10)
R→4398	0.7(3)	2.2(3)	0.81(11)	1.12(12)
R→4652	8.7(7)	6.8(3)	5.6(2)	5.25(18)
$E_r^{lab} = 193 \text{ keV}, E_r^{cm} = 183 \text{ keV} (J^\pi = 2^-)$				
Transition	Rolfs [44]	Di Leva [25]	present (coin)	present (sing)
R→0	–	2.9(4)	2.7(5)	2.8(6)
R→937	40(8)	24.5(8)	22.7(20)	24.0(20)
R→1042	–	3.4(4)	2.3(5)	2.5(6)
R→1081	60(8)	40.8(7)	44.1(18)	42.2(16)
R→2101	–	11.8(8)	10.0(8)	10.4(8)
R→2523	–	5.5(6)	6.5(7)	6.1(6)
R→3134	–	4.3(4)	4.2(5)	3.8(5)
R→3358	–	2.3(3)	2.3(4)	2.9(6)
R→3791	–	4.5(4)	5.2(5)	5.3(7)

^a Reported values add up to only 99.5%.

stronger 518 keV resonance (Sec. III B), there are two additional effects that must be taken into account in the analysis of the primary branching ratios and the total number of resonant reactions. First, compared to the $E_r^{lab} = 518 \text{ keV}$ resonance (Sec. III B), the strength of the $E_r^{lab} = 193 \text{ keV}$ resonance is smaller by almost four orders of magnitude, and therefore the derived numbers of partial $^{17}\text{O}+p$ reactions, N_i^{data} , have to be corrected for contributions from direct capture and tails of broad resonances (Sec. III D). This correction was performed

TABLE II. Strengths of low-energy resonances in $^{17}\text{O}(p,\gamma)^{18}\text{F}$.

$E_r^{lab} = 518 \text{ keV}, E_r^{cm} = 489 \text{ keV} (J^\pi = 4^-)$; units of $\omega\gamma$ in meV	
Rolfs [44] ^a	13.0 ± 2.5
Fox [15]	12 ± 3
Newton [20]	13.7 ± 2.2
Kontos [22]	13.0 ± 1.5
present (coin) ^b	12.9 ± 0.9
present (sing) ^b	14.5 ± 1.0
present (mean) ^c	13.7 ± 1.0
mean all values^d	13.3 ± 0.7
$E_r^{lab} = 193 \text{ keV}, E_r^{cm} = 183 \text{ keV} (J^\pi = 2^-)$; units of $\omega\gamma$ in μeV	
Fox [15]	1.2 ± 0.2
Chafa [16]	2.2 ± 0.4
DiLeva [25]	1.67 ± 0.12
present (coin) ^b	1.89 ± 0.14
present (sing) ^b	1.82 ± 0.13
present (mean) ^c	1.86 ± 0.13
mean all values^e	1.77 ± 0.09

^a Renormalized value, according to the suggestion of Ref. [15].

^b Systematic and statistical uncertainties are added in quadrature.

^c Mean value from singles and coincidence data of present work.

^d Recommended value, based on Refs. [15, 20, 22, 44] and the present mean value.

^e Recommended value, based on Refs. [16, 25] and the present mean value.

using the total S-factor measured in the present work (Sec. IIID and Tab. III). Second, angular correlations need to be considered since this 2^- p-wave resonance can be formed via channel spins of $j_s = 2$ or $j_s = 3$. An angular distribution of the 193 keV resonance in the corresponding (p,α) channel has been measured by Chafa et al. [17], with the result $W_{exp}(\theta) = 1 + (0.16 \pm 0.03)P_2(\cos\theta)$. For the theoretical angular distributions, we find $W_{theo}(\theta) = 1 - 0.70P_2(\cos\theta)$ for $j_s = 2$, and $W_{theo}(\theta) = 1 + 0.20P_2(\cos\theta)$ for $j_s = 3$. Consequently, the resonance is mainly formed via a channel spin of $j_s = 3$. With this value, the angular

correlations for transitions in $^{17}\text{O}(p,\gamma)^{18}\text{F}$ can be calculated for any given final state [40]. The angular correlation expressions have been included into our **Geant4** simulations.

Several templates were prepared for each measured spectrum: one template using the experimental room background, and ten $^{17}\text{O}+p$ templates simulated with **Geant4** for each of the observed primary transitions assuming known branching ratios for the subsequent *secondary* decays. The measured singles and coincidence spectrum was analyzed with the fraction fitter above an energy threshold of 1000 keV and 170 keV, respectively. The derived narrow-resonance primary branching ratios, both for our singles and the coincidence spectrum, are listed in Tab. I, and the values are in agreement. Our results overall agree with the recent study by Di Leva et al. [25].

From the number of $^{17}\text{O}+p$ reactions estimated by the fraction fitter, after correcting for non-resonant components, the resonance strength can be obtained from the thick-target yield since the total resonance width amounts only to 6 eV [17]. The statistical uncertainty determined by the fraction fitter amounts to 3.0%. The common uncertainties were already discussed in Sec. III B. Our measured resonance strengths are listed in Tab. II together with literature values. It can again be seen that the resonance strength values derived from our singles and coincidence spectra are in agreement. A test was performed by setting all angular correlations to isotropy. As a result, the total number of $^{17}\text{O}+p$ reactions obtained from the coincidence and singles spectrum increased by 0.7% and 1.2%, respectively. Our mean value amounts to $\omega\gamma_{pres}(193\text{ keV}) = (1.86 \pm 0.13) \times 10^{-6}$ eV. This result agrees with those reported by Chafa et al. [16] and Di Leva et al. [25] but exceeds the value of Fox et al. [15] significantly. We agree with the conjecture of Di Leva et al. [25] that the much lower statistics in the data of Fox et al. [15] precluded the observation of primary transitions except for the strongest two decays, and that this is the reason for the low resonance strength value of Ref. [15]. The weighted average of all measurements, excluding the value from Ref. [15], amounts to $\omega\gamma_{rec}(193\text{ keV}) = (1.77 \pm 0.09) \times 10^{-6}$ eV (Tab. II).

D. Total S-factor data for $^{17}\text{O}(p,\gamma)^{18}\text{F}$ at low energies

The total S-factor was measured at six laboratory bombarding energies: at 175 keV and 190 keV using the LENA ECRIS and at 250 keV, 275 keV, 300 keV, and 325 keV using the JN accelerator. Accumulated charges on target ranged from 3 C at the highest energy to

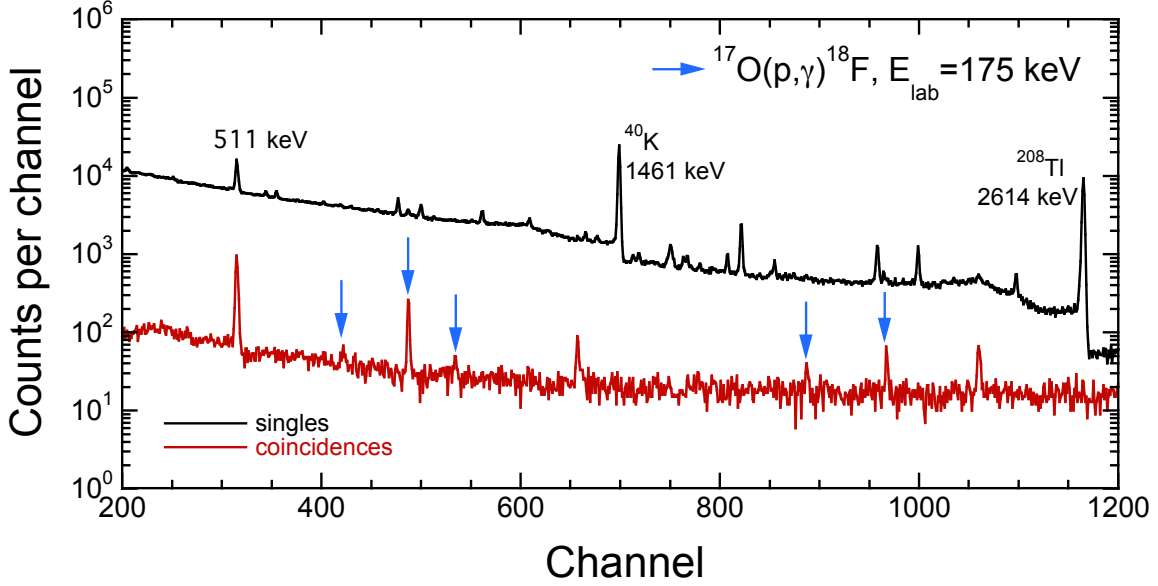


FIG. 4. (Color online) Singles (top) and coincidence (bottom) HPGe spectrum, measured at the lowest bombarding energy at $E_{lab} = 175$ keV. The HPGe-NaI(Tl) coincidence energy gate is given by Eq. (1). Peaks originating from the $^{17}\text{O}(p,\gamma)^{18}\text{F}$ reaction are marked by blue arrows. Unmarked peaks in the coincidence spectrum arise from the 511 keV annihilation radiation and the ^{18}O contamination in our target. The accumulated charge amounted to 100 C at a beam intensity of up to 2.0 mA.

100 C at the lowest energy. At the lowest measured energy, the expected yield is reduced by a factor of $\approx 10^5$ compared to the yield on top of the 518 keV resonance. Primary and secondary transitions from $^{17}\text{O}+p$ were observed at all measured energies.

Singles (black) and coincidence (red) spectra, measured at the lowest bombarding energy of $E_{lab} = 175$ keV, are displayed in Fig. 4. The accumulated charge amounted to 100 C at a beam intensity of up to 2.0 mA. This spectrum represents the data with the lowest signal-to-noise ratio. The coincidence condition of Eq. (1) reduces the background by about two orders of magnitude. Peaks originating from the $^{17}\text{O}(p,\gamma)^{18}\text{F}$ reaction are marked by blue arrows in the coincidence spectrum, and several of these peaks are either not observed or barely visible in the singles spectrum.

To determine which $^{17}\text{O}+p$ transitions are expected to predominate, we calculated partial S-factors by adding the resonant component, estimated from the Breit-Wigner equation together with measured resonant parameters from Ref. [22], to the expected direct capture

contribution, obtained from direct capture model calculations [46] that were scaled by measured spectroscopic factors [12, 22, 45]. There are 19 transitions with calculated primary branching ratios above 0.1%, and they are listed in Tab. III. These crudely estimated values of primary branching ratios did not enter in our data analysis in any way. Their only purpose was to identify the primary transitions for which $^{17}\text{O}+p$ templates had to be simulated using **Geant4**. Four more templates were simulated for contaminant reactions² ($^{11}\text{B}+p$, $^{14}\text{N}+p$, $^{18}\text{O}+p$, $^{19}\text{F}+p$). A measured room background spectrum served as the background template.

Angular correlations were computed for all primary transitions caused by the tails of higher-lying broad resonances and the direct capture process, including interferences between different amplitudes [21, 40]. The angular correlation expressions have been included into our **Geant4** simulations. We find that the primary source of an anisotropic radiation pattern in $^{17}\text{O}+p$ at low energies outside the region of the narrow resonances is the incoherent sum of the direct capture angular correlations arising from different bound state orbital angular momenta [21]. For more information, see Ref. [47].

To capture most of the decay strength, it is important to set the threshold for the spectral analysis as low in energy as possible. The coincidence spectra, with their superior signal-to-noise ratio, were analyzed with the fraction fitter above a threshold of 200 keV using a total of 23 templates. However, for the singles spectra, the fraction fitter did not converge below an energy of 2650 keV, presumably because the sensitivity was poor and too many transitions remained unobserved. For this reason, we extracted the S-factor almost exclusively from the coincidence data. At bombarding energies of ≥ 275 keV we could even extract the ground state transition strength from the coincidence data because the escape peaks were clearly observed. The singles spectra were analyzed with the fraction fitter above a γ -ray energy of 2650 keV only to extract the ground state transition at bombarding energies of ≤ 250 keV.

An impression of our analysis procedure can be obtained from Fig. 5, showing the decomposition of the measured coincidence spectrum (black line) at a bombarding energy of $E_{lab} = 250$ keV into the dominant simulated $^{17}\text{O}+p$ templates (green-blue lines). The measured room background template and the simulated beam-induced background templates are not displayed for reasons of clarity. The total simulated spectrum (i.e., sum of all simulated templates plus measured room background template) is shown as the red line. The good

² The beam-induced background was negligible for the narrow resonances discussed above.

agreement between measured and simulated data is apparent.

Our measured primary branching ratios are listed in Tab. III. First, we note that our experimental values are in overall agreement at the six measured energies. The data analysis was performed independently at the different energies, and therefore, this consistency supports our method of pulse height spectrum decomposition. We can also compare our measured primary branching ratios with the predicted values that were already mentioned above and are listed in column 2 of Tab. III. The overall agreement between measured and predicted values is reasonable. Therefore, we can use the predicted branching ratios to estimate the decay strength that is missing in our analysis because of the lower signal-to-noise ratio. At the three highest bombarding energies we miss at most a few percent of the primary decays. For the lower bombarding energies, the missing strength amounts to 8%, 11%, and 13% at $E_p^{lab} = 250, 190,$ and 175 keV, respectively. We do not adjust our total S-factor for any missing strength, because, first, the uncertainties of the crudely predicted branching ratios are difficult to quantify and, second, this correction would be smaller than our final experimental uncertainty in the S-factor at $E_{cm} = 0$ (see below). Table III also lists in the last column the primary branching ratios that were obtained by Di Leva et al. [25] at a laboratory bombarding energy near ≈ 320 keV ($E_{cm} = 301$ keV). Their values can be compared to our results measured at a bombarding energy of 325 keV (column 8 of Tab. III). It can be seen that the results are in agreement. However, at the lowest bombarding energy, near ≈ 175 keV, we measure the branching ratios of nine primary transitions, whereas only one primary decay (R/DC \rightarrow 937) is observed by Di Leva et al. [25] (see their Tab. I). For this reason, Ref. [25] extracted the total S-factor at this energy from their prompt γ -ray data using the 937 \rightarrow 0 secondary decay only and corrected the S-factor for an estimated missing decay strength of 30%. Their reported total S-factor amounts to 3.8 ± 0.6 keVb, which is significantly lower than the best fit using all of their data points (including the activation measurement; see their Fig. 8). Presumably there is still some missing decay strength that is not accounted for in the 175 keV prompt γ -ray data of Ref. [25].

From the total number of $^{17}\text{O}+p$ reactions, N_R^{data} , outside the region of the narrow resonances, the total cross section is calculated using the expression

$$Y(E_0) = \frac{N_R^{data}(E_0)}{N_p} = \int_{E_0-\Delta E}^{E_0} \frac{\sigma(E)}{\epsilon(E_0)} dE = \frac{\Delta(E_0)}{\epsilon(E_0)} \sigma(E_{eff}) f \quad (5)$$

where E_0 denotes the bombarding energy, ΔE is the target thickness in energy units, and

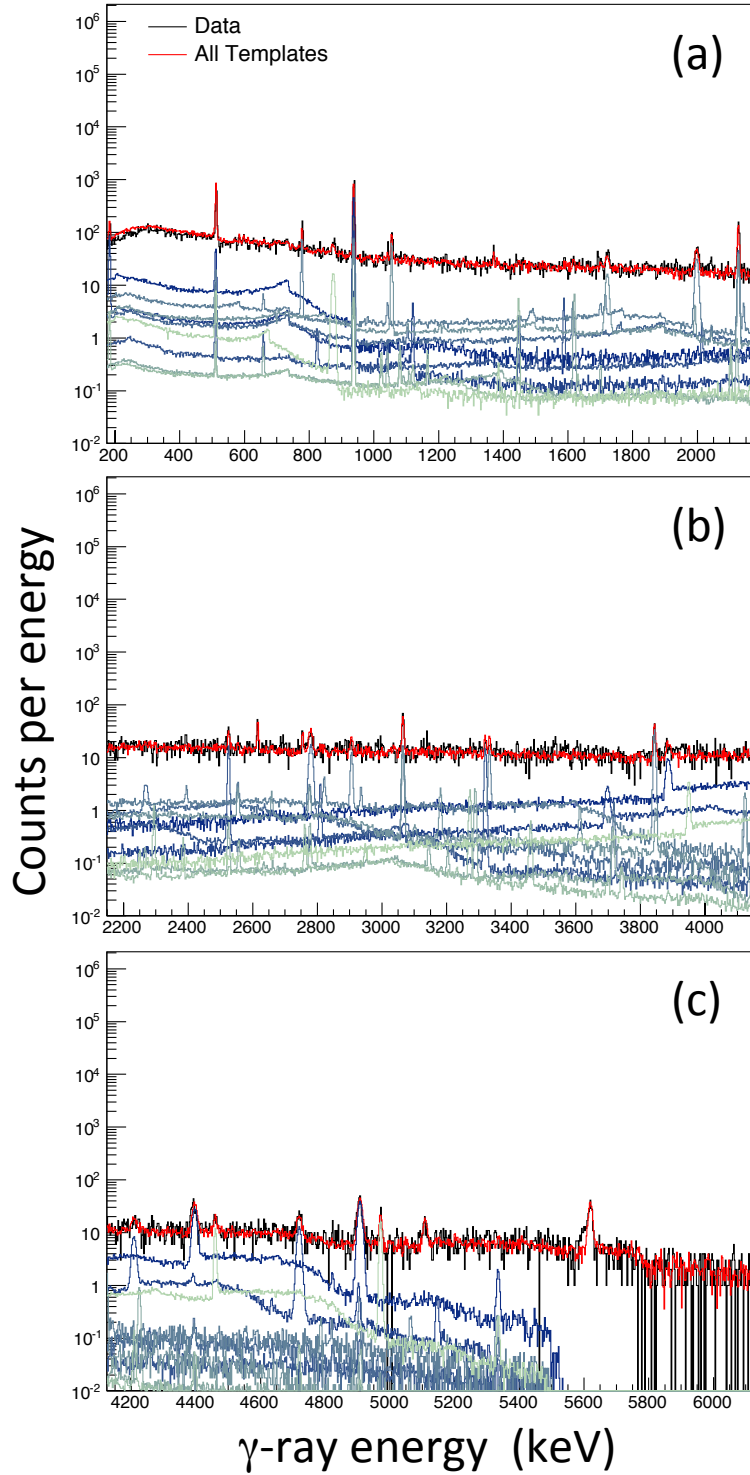


FIG. 5. (Color online) Decomposition of the measured coincidence spectrum (black line) at a bombarding energy of $E_{lab} = 250$ keV into the simulated $^{17}\text{O}+p$ templates (green-blue). The measured room background template and the simulated beam-induced background templates are not displayed for reasons of clarity. The total simulated spectrum (i.e., sum of all simulated and measured room background templates) is shown as the red line.

E_{eff} is the effective energy that accounts for the fact that most reactions occur at an energy smaller than the bombarding energy because of beam energy loss in the target. All quantities refer to the center-of-mass system. We assume that the effective stopping power is constant over the target thickness and that the energy dependence of the cross section is at most quadratic. Here we define the effective energy as the median energy, i.e., the energy at which half of the total yield is obtained. The resulting correction factor, f , is computed according to Brune and Sayre [48]. Finally, the total cross section at each bombarding energy is converted to the total S-factor, according to the definition $S(E) = Ee^{2\pi\eta}\sigma(E)$.

The results are listed at the bottom of Tab. III. The statistical uncertainty determined by the fraction fitter ranges from 2.6% at the highest bombarding energy of 325 keV to 9.1% at the lowest measured energy of 175 keV. Common uncertainties derive from the charge integration (3%), effective stopping power (4%), the simulation of HPGe and NaI(Tl) detection efficiencies using `Geant4` (5%), and the target thickness (2%). The latter uncertainty includes corrections for target degradation (Sec. II A). The uncertainties introduced by the cross section deconvolution procedure were negligible. A test was performed by setting all angular correlations to isotropy and, as a result, the total S-factor decreases by 11%. At a bombarding energy of 175 keV, our measured total S-factor (column 3) agrees with the crudely estimated value (column 2) within uncertainty.

Figure 6 shows our experimental total S-factor (red solid circles) together with literature values. The solid line is a fit of the present data alone, obtained by using the resonance properties of higher-lying resonances reported by Kontos et al. [22] and a constant direct capture S-factor as a free parameter. Our results are in excellent agreement with the prompt γ -ray measurement of Newton et al. [18] (green solid circles), which was performed with a single HPGe detector. The data points of Kontos et al. [22] and Hager et al. [23] lie systematically above the solid line, although their error bars are relatively large. The recent results of Di Leva et al. [25] are denoted by different symbols, depending on their method of measurement and analysis. Our total S-factors are in good agreement with their activation measurement (blue solid circles), although their two lowest-energy data points do not overlap with each other within their 1σ errors. Furthermore, their prompt γ -ray data points are either systematically higher (based on primary transitions only; blue open diamonds) or lower (based on secondary transitions only; blue open circles) compared to both their activation results and our (prompt γ -ray) data points.

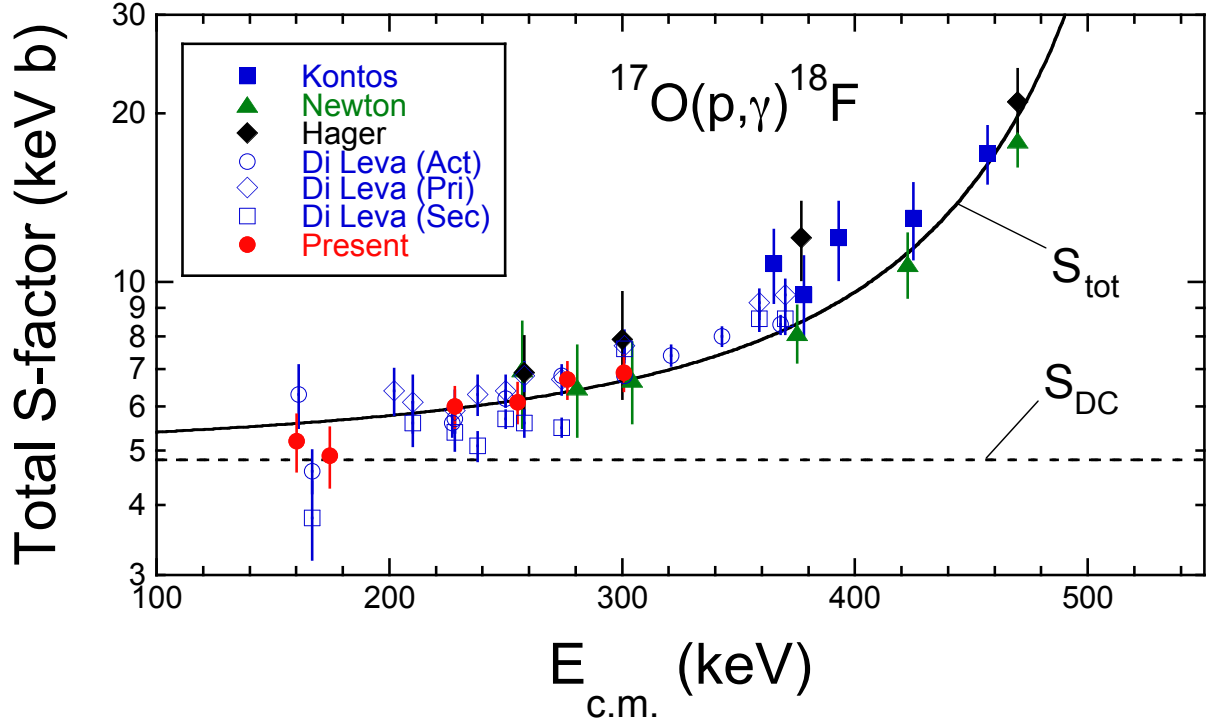


FIG. 6. (Color online) Total S-factor versus energy. Data point: (red) present work; (green) Newton et al. [18]; (black solid squares) Kontos et al. [22]; (black open squares) Hager et al. [23]; (blue) Di Leva et al. [25]; different symbols are used for the latter reference, according to the method (activation, primary transitions, secondary transitions). The results of Ref. [21] are disregarded because they disagree with all other measurements, and the single data point of Ref. [16] is not shown since its error (50%) is very large. The solid line shows the best fit of the total S-factor that is based on the present measurement alone, and the dashed line indicates the corresponding direct capture S-factor (see text).

The best fit value, based on our data alone, for the direct capture S-factor at zero energy (dashed line in Fig. 6) amounts to

$$S_{DC}^{pres}(0) = 4.82 \pm 0.41 \text{ keVb} \quad (6)$$

For the calculation of the thermonuclear reaction rates (Sec. IV A), we averaged the results from all measurements, except for the S-factors reported by Rolfs [21] and Chafa et al. [16]. The former results disagree with all other measurements, while the single data point from the latter work has a very large error (50%).

IV. THERMONUCLEAR REACTION RATES OF $^{17}\text{O}(p,\gamma)^{18}\text{F}$ AND $^{17}\text{O}(p,\alpha)^{14}\text{N}$

Experimental thermonuclear rates of the $^{17}\text{O}+p$ reactions are calculated using the code `RatesMC` [49], which is based on the random sampling using the Monte Carlo procedure presented in Longland et al. [50]. The total thermonuclear rate (in units of $\text{cm}^3 \text{mol}^{-1} \text{s}^{-1}$) for a reaction involving two nuclei 0 and 1 in the entrance channel, at a given temperature T , is given by

$$N_A \langle \sigma v \rangle_{01} = \frac{3.7318 \cdot 10^{10}}{T_9^{3/2}} \sqrt{\frac{M_0 + M_1}{M_0 M_1}} \int_0^\infty E \sigma(E) e^{-11.605 E/T_9} dE \quad (7)$$

where the center-of-mass energy, E , is in units of MeV, the temperature, T_9 , is in GK ($T_9 \equiv T/10^9 \text{ K}$), the atomic masses, M_i , are in u, and the cross section, σ , is in barn ($1 \text{ b} \equiv 10^{-24} \text{ cm}^2$); N_A denotes Avogadro's constant. In this section, all energies refer to the center-of-mass coordinate system. The reaction rate is determined by the absolute magnitude and the energy dependence of the nuclear reaction cross section, $\sigma(E)$. Based on the energy-dependence of $\sigma(E)$, a number of different specialized expressions and procedures can be derived for certain contributions to the total reaction rate. These expressions can be found, for example, in Ref. [40] and will not be repeated here.

We will briefly point out the nuclear physics input required for the Monte Carlo rate calculations. For a non-resonant process, the astrophysical S-factor varies slowly with energy. The non-resonant S-factor is usually expanded into a power series, and the input to the rate calculation consists of the value and the slope of $S(E)$ at zero bombarding energy. The probability density functions of these quantities, assumed to be described by a lognormal distribution, can be computed using uncertainties derived from the measured data (see Sec. 5.1.3 of Ref. [50]). For resonances, the Breit-Wigner equation can be substituted into Eq. (7). The integral can only be solved numerically if all three partial widths (Γ_p , Γ_α , Γ_γ) are known for a given resonance. Frequently, resonances are *narrow*, in the sense that their cross section can not be obtained experimentally. All that is measured in this case is the resonance strength, which is proportional to the resonance integral. The narrow resonance reaction rate can be obtained analytically and depends linearly on the resonance strength and exponentially on the resonance energy. The disadvantage of using the analytical expression derives from the fact that it does not account for the resonance tail contributions. Therefore, when all three partial widths are known, it is usually safer to compute the resonance reaction

rates via numerical integration of Eq. (7). Nevertheless, in exceptional cases we used the narrow-resonance analytical approximation. This is discussed in more detail below since it has caused some misunderstanding in the recent literature. For the random sampling, we assume a Gaussian probability density for resonance energies and lognormal densities for resonance strengths or partial widths. All probability density functions are computed using experimental uncertainties, as explained in Ref. [50].

Random samples are calculated for all nuclear physics input quantities (non-resonant cross section, resonance energies and strengths, reduced width upper limits, etc.), and a total rate sample is obtained from Eq. (7) (or its approximations). The procedure is repeated 10,000 times, providing the probability density of the total reaction rate. It is used to derive a recommended reaction rate and rate uncertainties based on a desired coverage probability (e.g., 68% or 95%). The current version of `RatesMC` (v. 2.8) is applicable to any nuclear reaction provided that the total rates are determined by the incoherent contributions of any number of broad or narrow resonances and by up to two non-resonant (i.e., direct) amplitudes. The code also accounts for interferences between any two resonant amplitudes. Interferences between more than two resonant contributions or between a resonant and a non-resonant amplitude have not been implemented yet. These extensions are not needed for calculating the $^{17}\text{O}+p$ rates.

We calculate the rates by taking into account all of the published experimental results. Details on the nuclear physics input are provided below. Except where noted otherwise, all resonance energies are obtained from experimental ^{18}F excitation energies listed in Ref. [51], and the most recent value of the proton separation energy, $S_p = 5607.1 \pm 0.5$ keV [52], which differs from the previous value [53] by 0.6 keV.

A. Direct Capture in $^{17}\text{O}(p,\gamma)^{18}\text{F}$

Direct capture S-factors derived from measurements are reported in Refs. [20, 22, 23, 25]. Together with the present result (Sec. III D), the weighted average amounts to $S_{DC}^{rec}(0) = 4.9 \pm 0.3$ keV. The R-matrix analysis of Kontos et al. [22] provides a value for the small energy dependence (see their Fig. 9). Thus we adopt the following expression for the direct capture S-factor:

$$S_{DC}(E) = 4.9 + 1.19 \times 10^{-3} E \ (\pm 6.3\%) \ (\text{keV b}) \quad (8)$$

This expression should be accurate at least up to a bombarding energy of $E^{cm} \approx 2.0$ MeV (see Fig. 9 of Ref. [22]). In the absence of more information, we extrapolate the above expression to higher energies to compute the direct capture rate contribution up to temperatures of 10 GK.

The direct capture S-factor adopted here disagrees both in magnitude and in energy dependence with the results of Rolfs [21] (see his Fig. 17) and Rolfs and Rodney [10] (see their Fig. 3).

B. Subthreshold 1^+ resonance at $E_r^{cm} = -3.7$ keV

This subthreshold resonance corresponds to the ^{18}F level at an excitation energy of $E_x = 5603.38 \pm 0.27$ keV. The measured α -particle and γ -ray partial widths amount to $\Gamma_\alpha = 42.8 \pm 1.6$ eV and $\Gamma_\gamma = 0.485 \pm 0.046$ eV, respectively [54]. To compute the contributions to the (p,γ) and (p,α) reaction rates by numerically solving Eq. (7), an estimate for the proton spectroscopic factor is required. We adopt the value of $C^2S = 0.12 \pm 0.04$ from Landre et al. [12], which was obtained by measuring the $^{17}\text{O}(^3\text{He,d})^{18}\text{F}$ transfer reaction.

This value is in strong disagreement with the result reported from the direct capture work of Rolfs and Rodney [10], who report $C^2S < 0.002$. Thus we suspect that upper limit values on C^2S obtained by Ref. [10] for other levels may also be questionable (see below).

C. Interfering 1^- resonances at $E_r^{cm} = -2.2$ keV and 65 keV

The subthreshold resonance corresponds to the ^{18}F level at $E_x = 5604.86 \pm 0.28$ keV. The measured α -particle and γ -ray partial widths amount to $\Gamma_\alpha = 32.0 \pm 2.1$ eV and $\Gamma_\gamma = 0.891 \pm 0.074$ eV, respectively [54]. This level is only weakly populated in the $^{17}\text{O}(^3\text{He,d})^{18}\text{F}$ transfer work of Landre et al. [12], who obtain an upper limit of $C^2S < 0.020$. We adopt this result instead of the much smaller value of Rolfs and Rodney [10], $C^2S < 0.0003$, which could prove unreliable considering the disagreement noted in Sec. IV B. Since only an upper limit is available for the proton spectroscopic factor (or the reduced width), its value is randomly sampled using a Porter-Thomas distribution, as explained in Ref. [50]. For the required mean reduced width we estimate a value of $\langle \theta_p^2 \rangle = 0.0050 \pm 0.0025$ based on the analysis presented in Pogrebnyak et al. [56].

The lowest-lying (above proton threshold) energy resonance corresponds to a ^{18}F level at $E_x = 5671.6 \pm 0.2$ keV. This value was obtained in the extensive work of Chafa et al. [17] and results in a resonance energy of $E_r^{cm} = 64.5 \pm 0.5$ keV, where the quoted uncertainty is dominated by the proton separation energy. Three resonance properties have been measured for this resonance: the (p,α) resonance strength, $\omega\gamma_{p\alpha} = (4.7 \pm 0.8) \times 10^{-9}$ eV [13, 55]; the (α,γ) resonance strength, $\omega\gamma_{\alpha\gamma} = 0.44 \pm 0.02$ eV [44, 57–59]; and the α -particle partial width, $\Gamma_\alpha = 130 \pm 5$ eV [54]. Solving for the individual partial widths, we find values of $\Gamma_p = (19.0 \pm 3.2) \times 10^{-9}$ eV, $\Gamma_\alpha = 130 \pm 5$ eV, and $\Gamma_\gamma = 0.44 \pm 0.02$ eV.

These two 1^- resonances are expected to interfere in their total S-factor. We find the coherent sum of their contributions to the (p,γ) and (p,α) reaction rates by numerically solving Eqs. (18) and (19) of Ref. [50]. Since the interference sign is unknown, we assume a binary probability density in the random sampling (Sec. 4.4 of Ref. [50]).

D. Resonance at $E_r^{cm} = 183$ keV (2^-)

Fox et al. [15] report a directly measured excitation energy of $E_x = 5788.9 \pm 1.0$ keV, while Chafa et al. [17] find a value of $E_x = 5789.8 \pm 0.3$ keV. The laboratory resonance energy has also been measured directly by Ref. [15], yielding $E_r^{lab} = 193.3 \pm 1.5$ keV. The weighted mean of these results give a center-of-mass resonance energy of $E_r^{cm} = 182.6 \pm 0.5$ keV.

The (p,γ) resonance strength has been discussed in Sec. III C. The weighted mean value, including the present measurement, amounts to $\omega\gamma_{rec}(193 \text{ keV}) = (1.77 \pm 0.09) \times 10^{-6}$ eV (Tab. II). Values for the (p,α) resonance strength are reported in Refs. [16–19]. All of the results are in agreement, and we adopt an average value of $\omega\gamma_{p\alpha} = (1.66 \pm 0.13) \times 10^{-3}$ eV.

The (α,γ) resonance strength for this compound level has been measured by Rolfs, Charlesworth and Azuma [44], who report a value of $\omega\gamma_{\alpha\gamma} = 0.016 \pm 0.006$ eV. From the three measured resonance strengths, the partial widths Γ_p , Γ_α , and Γ_γ can be derived, and the reaction rate contribution can be obtained numerically using Eq. (7). This procedure, which automatically takes the resonance tail contributions into account, was followed by Iliadis et al. [8]. The disadvantage is that the 40% uncertainty on the $\omega\gamma_{\alpha\gamma}$ value propagates to relatively large uncertainties in Γ_α and Γ_γ . Random sampling over the partial widths thus results in much larger (p,γ) and (p,α) reaction rate uncertainties compared to randomly sampling over the resonance energy and strength (i.e., when using the analytical

narrow-resonance expression; see Eq. (10) of Ref. [50]). We performed a number of tests and find that the tails of the 183 keV resonance are negligible for the total reaction rate. Therefore, we follow the suggestion of Di Leva et al. [25] and calculate the rate contribution of this resonance using the narrow resonance formalism.

E. Resonance at $E_r^{cm} = 489$ keV (4^-)

The resonance corresponds to a ^{18}F level at an excitation energy of $E_x = 6096.4 \pm 1.1$ keV. The laboratory bombarding energy amounts to $E_r^{lab} = 518$ keV, and we discussed this resonance in Sec. III B. Its (p,γ) resonance strength is important since it allows for a consistency check of strengths of higher-lying resonances that have been measured by different groups. The weighted average of all consistent measurements, including the present work, amounts to $\omega\gamma_{rec}(518 \text{ keV}) = (13.3 \pm 0.7) \times 10^{-3}$ eV (Tab. II). The rate contribution is found using the narrow resonance formalism.

For the (p,α) reaction, values of the partial widths Γ_p and Γ_α are presented in the R-matrix analysis of Kieser et al. [11], and we calculate the rate contribution by numerical integration of Eq. (7).

F. Resonances at $E_r^{cm} = 556$ keV (3^+) and 676 keV (2^+)

These two resonances correspond to ^{18}F levels at $E_x = 6163.2 \pm 0.9$ keV and 6283.2 ± 0.9 keV. Values for the partial widths, Γ_p , Γ_α , and Γ_γ , are adopted from the R-matrix analysis of Kontos et al. [22]. The derived values agree with their directly measured (p,γ) resonance strengths. We inflated the reported tiny uncertainties of the γ -ray partial widths ($\approx 1\%$) to match the uncertainties in their $\omega\gamma_{p\gamma}$ values ($\approx 12\%$). The (p,γ) and (p,α) rate contributions are found by numerically integrating Eq. (7).

G. Other higher-lying resonances with $E_r^{cm} \geq 501$ keV

For higher-lying resonances in the (p,γ) reaction, the resonance strengths are adopted from the weighted average of the renormalized values of Rolfs [21] and the results of Kontos et al. [22]. We again disregard the older values of Ref. [43]. The contributions of the higher-

lying resonances are computed using the narrow resonance expression (Eq. (10) of Ref. [50]). The highest lying resonance for which reliable strength values are available is located at $E_r^{cm} = 1270$ keV.

For the (p,α) reaction, the partial widths Γ_p and Γ_α are obtained from the R-matrix analysis of Kieser et al. [11]. These rate contributions are found by numerically integrating Eq. (7). We take resonances up to an energy of $E_r^{cm} = 1684$ keV into account.

H. Total (p,γ) and (p,α) reaction rates

The total $^{17}\text{O}+p$ reaction rates are shown in Fig. 7. The displayed rates are normalized to the present recommended (median) rates. The shading indicates the coverage probability in percent (see legend on right-hand side). Thick and thin solid black lines depict the high and low Monte Carlo rates corresponding to a coverage probability of 68% and 95%, respectively. For both the (p,γ) and (p,α) reaction, the maximum rate uncertainties occur below a temperature of 100 MK. In this region, they amount to factors of ≈ 1.35 (1.15) based on a coverage probability of 95% (68%). Numerical values of our new reaction rates, including uncertainties, probability densities, and the entire nuclear physics input, can be found on the website <http://starlib.physics.unc.edu>.

The Monte Carlo based method also allows for an estimation of the fractional contributions of individual resonances to the total $^{17}\text{O}+p$ reaction rates. Results are shown in Fig. 8. Different contributions are marked by color and the vertical width of each band corresponds to a coverage probability of 68%. The dotted black line shows contributions of resonances with energies in excess of 1270 keV and 1684 keV in the (p,γ) and (p,α) channel, respectively

In the $^{17}\text{O}(p,\gamma)^{18}\text{F}$ reaction, the direct capture process provides the largest rate contribution at most temperatures, except at 20–90 MK and at 0.35–5 GK, where the resonances at 65 keV and 556 keV, respectively, dominate the total rate. The resonances at 183 keV, 529 keV, and 676 keV contribute significantly at temperatures above 100 MK, although they never dominate the total rate. The dominance of the direct capture process also at very high temperatures, $T > 5$ GK, is striking and reflects the absence of strong resonances at higher bombarding energies, as can best be seen from Fig. 11 of Ref. [21]. In the $^{17}\text{O}(p,\alpha)^{14}\text{N}$ reaction, the resonances at 65 keV, 183 keV, 489 keV, and 1202 keV dominate the total rates at all temperatures in excess of 13 MK. Above a temperature of 2 GK, the (p,α) rates need to be

corrected for unobserved resonance contributions. This correction has been performed using results obtained from the Hauser-Feshbach code TALYS, following the procedure outlined in Ref. [60].

The ratio of (p,α) and (p,γ) reaction rates versus stellar temperature is displayed in Fig. 9. It can be seen that the (p,α) rate dominates over the competing (p,γ) rate at all temperatures. Except at $T \leq 20$ MK, the reaction rate ratio exceeds an order of magnitude.

Our results are compared to the 2010 reaction rate evaluation [8] in Fig. 10. The ratio of previous and present *recommended* rates is shown as solid black lines. For the $^{17}\text{O}(p,\gamma)^{18}\text{F}$ reaction (part a), our rates are higher by up to 20% for temperature below 3 GK. Our much higher rates at elevated temperatures (by a factor of 4 at 10 GK) are caused by the fact that the direct capture rate was artificially cut off by Ref. [8] at an energy of 1.2 MeV, whereas here we take the full direct capture S-factor into account (Sec. IV A). Except at $T = 40\text{--}60$ MK, our rate uncertainties (grey shaded area) are smaller than those of Ref. [8] (blue shaded area) at almost all temperatures. This is caused by the improved knowledge of the direct capture S-factor (Sec. IV A), the analytic calculation of the 183 keV resonance contribution (Sec. IV D), and the improved strengths of higher-lying resonances (Sec. IV G). Our (p,γ) rates are in overall agreement with the recent results of Di Leva et al. [25], with a maximum deviation of $\approx 20\%$ near 30 MK.

For the $^{17}\text{O}(p,\alpha)^{14}\text{N}$ reaction (part b), the present and previous [8] rate uncertainties are very similar. The recommended rates deviate by $\approx 30\%$ near 20 MK and by $\approx 50\%$ at 10 GK. The deviation at low temperatures is caused by the higher adopted upper limit for the spectroscopic factor of the -2 keV subthreshold resonance (Sec. IV C), while the deviation at the highest temperatures is caused by the fact that we use a different Hauser-Feshbach prescription (TALYS versus NON-SMOKER) compared to Ref. [8] in order to account for missing resonance contributions.

V. SUMMARY AND CONCLUSIONS

We measured the $^{17}\text{O}(p,\gamma)^{18}\text{F}$ reaction in the laboratory energy range of 170 – 530 keV, with an unprecedented maximum beam current of $I_{max} \approx 2$ mA. We also measured the cross section at much lower energies compared to previous in-beam experiments. For the first time in this reaction, a sophisticated γ -ray coincidence spectrometer, consisting of a

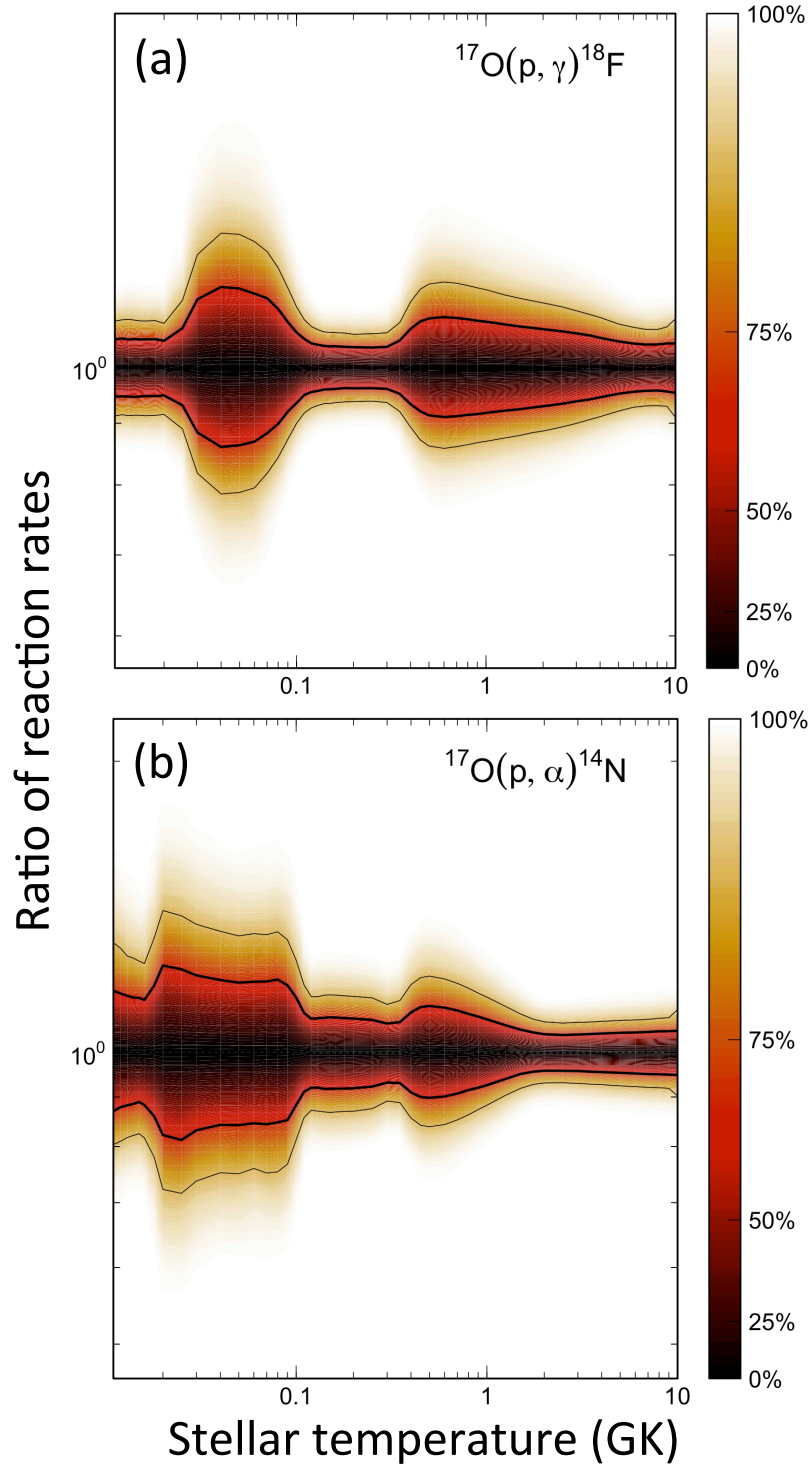


FIG. 7. (Color online) Contour plots of Monte Carlo based total reaction rates for (a) $^{17}\text{O}(p,\gamma)^{18}\text{F}$, and (b) $^{17}\text{O}(p,\alpha)^{14}\text{N}$. For a better comparison, all rates are normalized to the present recommended (median) rates. The shading indicates the coverage probability in percent (see legend on right-hand side). The thick (thin) black lines indicate the high and low Monte Carlo rates for a coverage probability of 68% (95%).

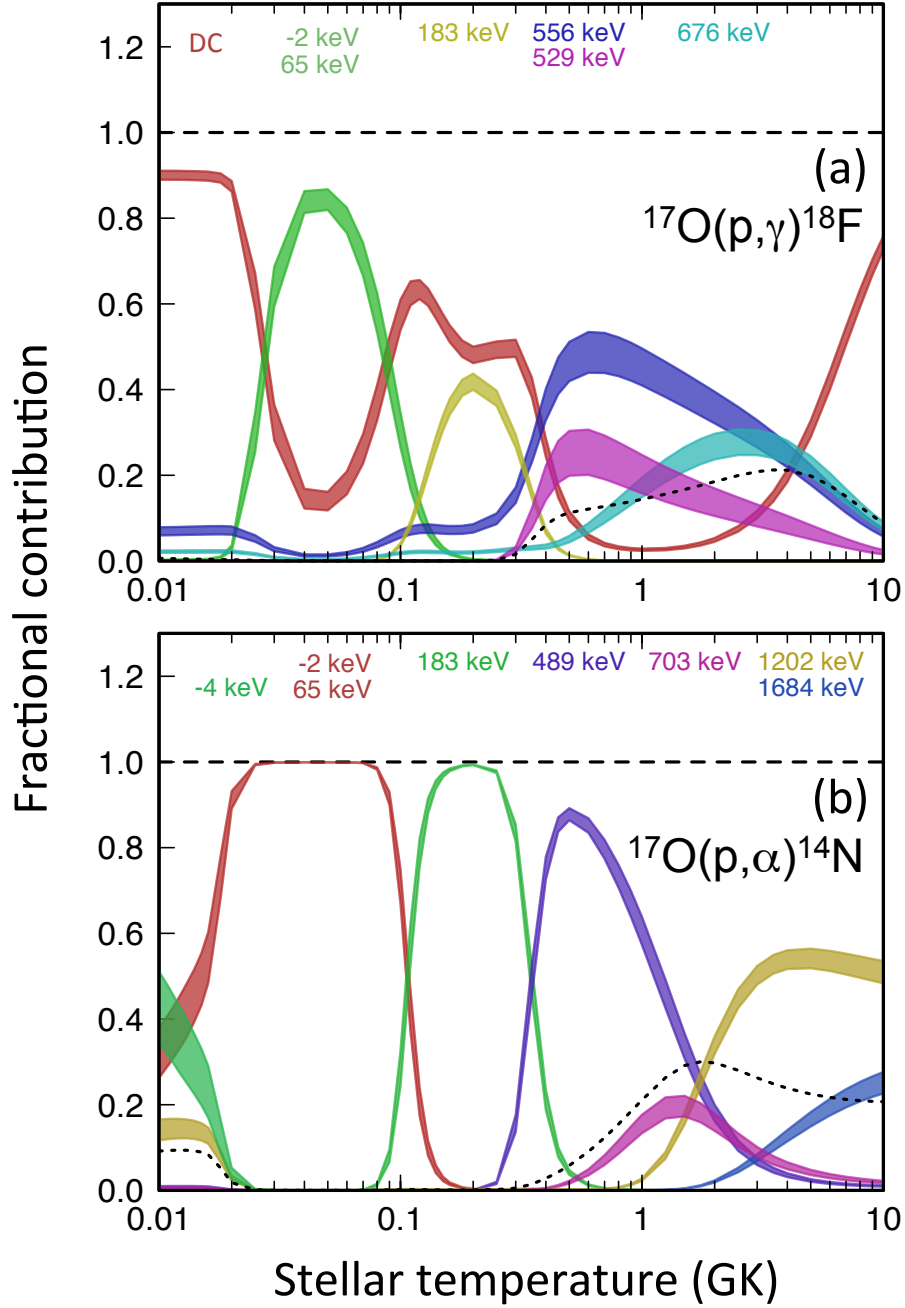


FIG. 8. (Color online) Fractional contributions to the total reaction rates of (a) $^{17}\text{O}(p,\gamma)^{18}\text{F}$, and (b) $^{17}\text{O}(p,\alpha)^{14}\text{N}$. Different colors denote different contributions. The vertical width of a band indicates the Monte Carlo uncertainty of a fractional contribution and corresponds to a coverage probability of 68%. Numbers at the top denote center-of-mass energies of given resonances. For the interfering -2.2 keV and 65 keV resonances, only their total coherent contribution is shown. The dotted black line shows contributions of resonances with energies larger than 1270 keV and 1684 keV in the (p,γ) and (p,α) channel, respectively.

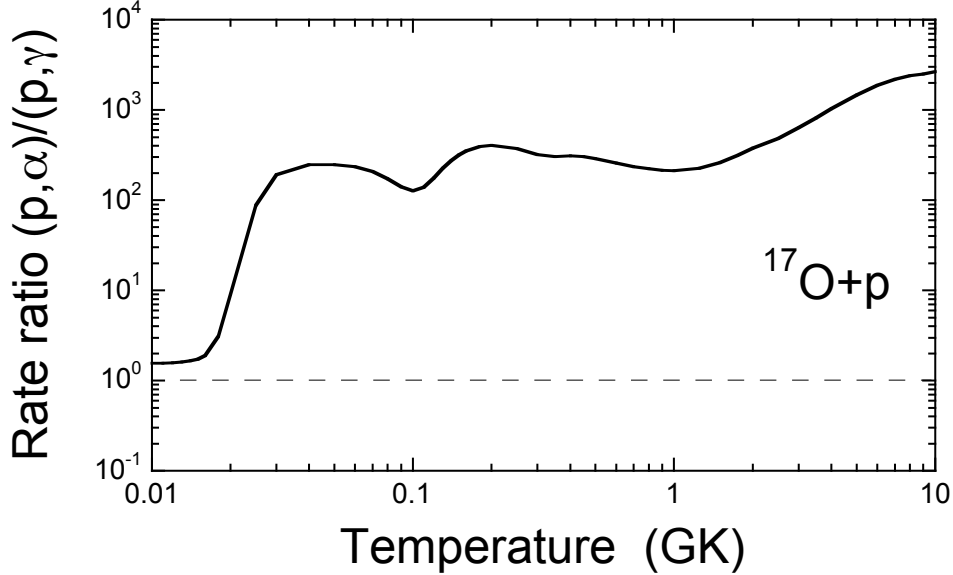


FIG. 9. Ratio of $^{17}\text{O}(p,\alpha)^{14}\text{N}$ and $^{17}\text{O}(p,\gamma)^{18}\text{F}$ recommended (median) Monte Carlo reaction rates versus stellar temperature.

large-volume HPGe detector and a NaI(Tl) annulus, is employed. The substantial increase in detection sensitivity allowed for a novel data analysis method that relies on a decomposition of the complete HPGe coincidence spectrum into different components arising from various primary decays in $^{17}\text{O}+p$. We demonstrated that our method gives consistent results for the strengths of the low-energy resonances at bombarding energies of 193 keV and 518 keV compared to the most sensitive previous measurements. With regard to the low-energy S-factor, our data contain, unlike previous prompt γ -ray studies, almost the entire decay strength in $^{17}\text{O}+p$. Thus our data points scatter much less than previous results. Based on the present measurement and all consistent previous studies, we present new thermonuclear reaction rates for the $^{17}\text{O}(p,\gamma)^{18}\text{F}$ and $^{17}\text{O}(p,\alpha)^{14}\text{N}$ reactions that will allow for more reliable simulations of low-mass stars and classical novae.

ACKNOWLEDGMENTS

This work was supported in part by the U.S. Department of Energy under Contract No. DE-FG02-97ER41041. Additional support was provided for MQB by the DOE NNSA SSGF

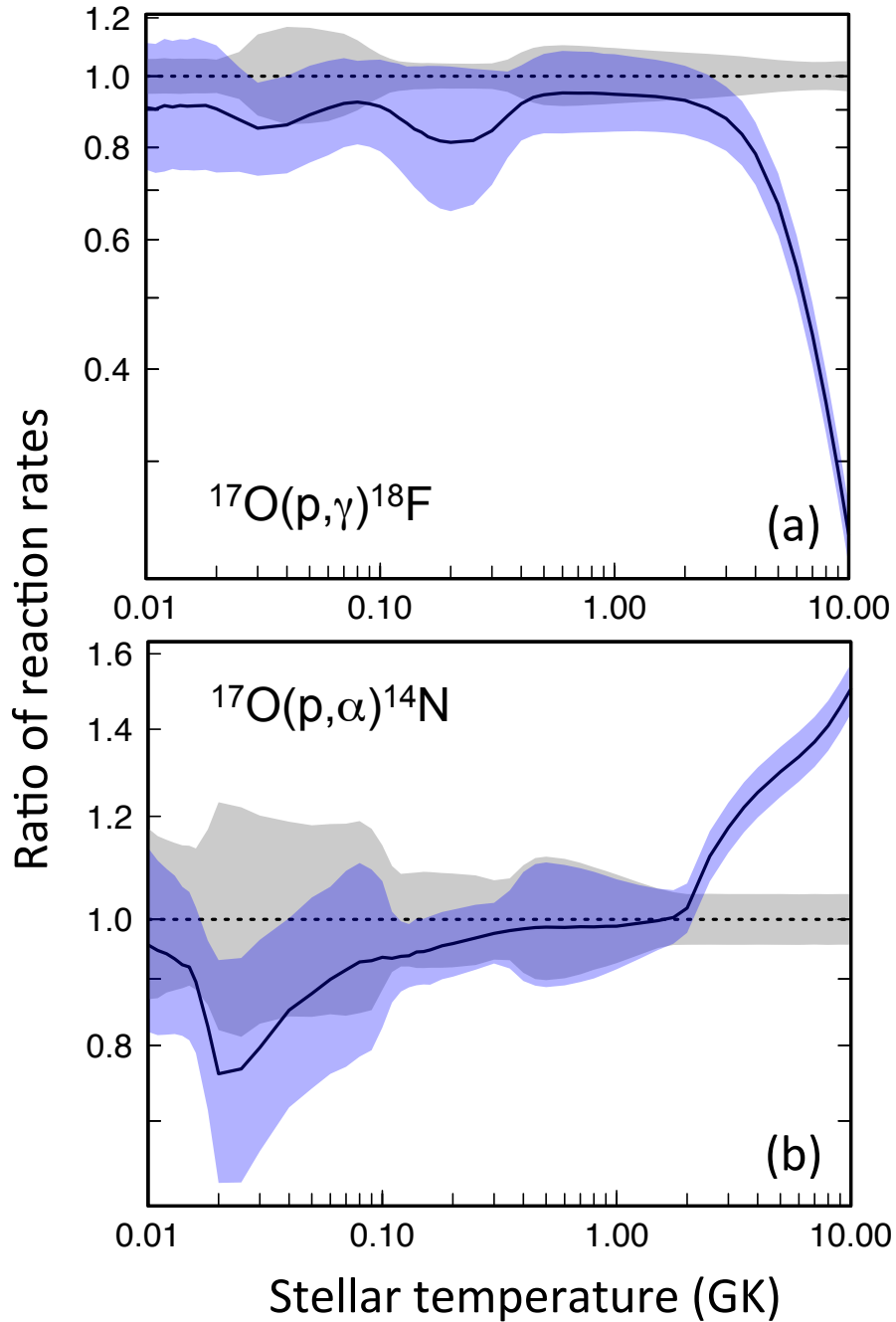


FIG. 10. (Color online) Reaction rate comparison of present results with a recent evaluation [8] for (a) $^{17}\text{O}(p,\gamma)^{18}\text{F}$, and (b) $^{17}\text{O}(p,\alpha)^{14}\text{N}$. The grey shaded area corresponds to the new Monte Carlo-based rates, while the blue shaded area depicts the previous rates. The bands signify a 68% coverage probability. All rates are normalized to the new recommended rate. The solid line shows the ratio of previous and present recommended rates.

under Grant No. DE-FC52-08NA28752.

- [1] A.I. Boothroyd and I.-J. Sackman, *Astrophys. J.* 510, 232 (1999).
- [2] F. Herwig, *Annu. Rev. Astron. Astrophys.* 43, 435 (2005).
- [3] A.I. Boothroyd, I.-J. Sackman and G.J. Wasserburg, *Astrophys. J. Lett.* 442, 21 (1995).
- [4] J. José, M. Hernanz and C. Iliadis, *Nucl. Phys. A* 777, 550 (2006).
- [5] T. Tsuji, *Astron. Astrophys.* 489, 1271 (2008).
- [6] B.S. Meyer, L.R. Nittler, A.N. Nguyen and S. Messenger, *Rev. Mineral. Geochem.* 68, 31 (2008).
- [7] C. Iliadis, C. Angulo, P. Descouvemont, M. Lugaro and P. Mohr, *Phys. Rev. C* 77, 045802 (2008).
- [8] C. Iliadis, R. Longland, A.E. Champagne, A. Coc and R. Fitzgerald, *Nucl. Phys. A* 841, 31 (2010).
- [9] M.Q. Buckner, C. Iliadis, J.M. Cesaratto, C. Howard, T.B. Clegg, A.E. Champagne and S. Daigle, *Phys. Rev. C* 86, 065804 (2012).
- [10] C. Rolfs and W.S. Rodney, *Nucl. Phys. A* 250, 295 (1975).
- [11] W.E. Kieser, R.E. Azuma and K.P. Jackson, *Nucl. Phys. A* 331, 155 (1979).
- [12] V. Landre et al., *Phys. Rev. C* 40, 1972 (1989).
- [13] J.C. Blackmon et al., *Phys. Rev. Lett.* 74, 2642 (1995).
- [14] C. Fox et al., *Phys. Rev. Lett.* 93, 081102 (2004).
- [15] C. Fox et al., *Phys. Rev. C* 71, 055801 (2005).
- [16] A. Chafa et al., *Phys. Rev. Lett.* 95, 031101 (2005).
- [17] A. Chafa et al., *Phys. Rev. C* 75, 035810 (2007).
- [18] J. R. Newton, C. Iliadis, A. E. Champagne, R. Longland and C. Ugalde, *Phys. Rev. C* 75, 055808 (2007).
- [19] B. H. Moazen et al., *Phys. Rev. C* 75, 065801 (2007).
- [20] J.R. Newton et al., *Phys. Rev. C* 81, 045801 (2010).
- [21] C. Rolfs, *Nucl. Phys. A* 217, 29 (1973).
- [22] A. Kontos et al., *Phys. Rev. C* 86, 055801 (2012).
- [23] U. Hager et al., *Phys. Rev. C* 85, 035803 (2012).

- [24] D.A. Scott et al., Phys. Rev. Lett. 109, 202501 (2012).
- [25] A. Di Leva et al., Phys. Rev. C 89, 015803 (2014).
- [26] J.M. Cesaratto, A.E. Champagne, T.B. Clegg, M.Q. Buckner, R.C. Runkle and A. Stefan, Nucl. Instr. Meth. A 623, 888 (2010).
- [27] H.W. Becker et al., Z. Phys. A 351, 453 (1995).
- [28] M. Uhrmacher et al., Nucl. Instr. Meth. B 9, 234 (1985).
- [29] D. Phillips and J.P.S. Pringle, Nucl. Instr. Meth. 135, 389 (1976).
- [30] C. Rowland et al., Nucl. Instr. Meth. A 480, 610 (2002).
- [31] F. Ajzenberg-Selove, Nucl. Phys. A 523, 1 (1991).
- [32] R. Longland et al., Nucl. Instr. Meth. A 566, 452 (2006).
- [33] K.B. Swartz, D.W. Visser and J.M. Baris, Nucl. Instr. Meth. A 463, 354 (2001).
- [34] D.R. Tilley, H.R. Weller, C.M. Cheves and R.M. Chasteler, Nucl. Phys. A 595, 1 (1995).
- [35] S. Agostinelli et al., Nucl. Instr. Meth. 506, 250 (2003).
- [36] J. Allison et al., IEEE Trans. Nucl. Sci. NS-53, 270 (2006).
- [37] S. Carson et al., Nucl. Instr. Meth. A 618, 190 (2010).
- [38] C. Howard, C. Iliadis and A.E. Champagne, Nucl. Instr. Meth. A 729, 254 (2013).
- [39] J.M. Cesaratto et al., Phys. Rev. C 88, 065806 (2013).
- [40] C. Iliadis, *Nuclear Physics of Stars* (Wiley-VCH, Weinheim, 2007).
- [41] R. Barlow and C. Beeston, Comp. Phys. Comm. 77, 219 (1993).
- [42] R. Brun and F. Rademakers, Nucl. Instr. Meth. A 389, 81 (1997).
- [43] J.C. Sens, A. Pape and R. Armbruster, Nucl. Phys. A 199, 241 (1973).
- [44] C. Rolfs, A.M. Charlesworth and R.E. Azuma, Nucl. Phys. A 199, 257 (1973).
- [45] L.M. Polsky, C. Holbrow and R. Middleton, Phys. Rev. 186, 966 (1969).
- [46] C. Iliadis and M. Wiescher, Phys. Rev. C 69, 064305 (2004).
- [47] M.Q. Buckner, PhD thesis (University of North Carolina at Chapel Hill, 2014).
- [48] C. Brune and D.B. Sayre, Nucl. Instr. Meth. A 698, 49 (2013).
- [49] <http://starlib.physics.unc.edu>.
- [50] R. Longland et al., Nucl. Phys. A 841, 1 (2010).
- [51] <http://www.nndc.bnl.gov/ensdf/>.
- [52] M. Wang et al., Chinese Physics C 36, 1603 (2012).
- [53] G. Audi, A. H. Wapstra and C. Thibault, Nucl. Phys. A729, 337 (2003).

- [54] H.B. Mak, G.T. Ewan, H.C. Evans, J.D. MacArthur and W. McLatchie, Nucl. Phys. A343, 79 (1980).
- [55] M.D. Hannam and W.J. Thompson, Nucl. Instr. Meth. A 431, 239 (1999).
- [56] I. Pogrebnyak, C. Howard, C. Iliadis, R. Longland and G.E. Mitchell, Phys. Rev. C 88, 015808 (2013).
- [57] P.D. Parker, Phys. Rev. 173, 1021 (1968).
- [58] I. Berka et al., Nucl. Phys. A 288, 317 (1977).
- [59] H.W. Becker et al., Z. Phys. A 305, 319 (1982).
- [60] A.L. Sallaska et al., Astrophys. J. Suppl. 207, 18 (2013).

TABLE III. Measured primary branching ratios and total S-factors in $^{17}\text{O}(p,\gamma)^{18}\text{F}$. All listed values are from the present experiment, except those in square parenthesis.

Transition ^a	Primary branching ratios ^b (%) at E_p^{lab} (keV)							
	175 ^c	175	190	250	275	300	325	$\approx 320^e$
R/DC \rightarrow 0	[4.2]	–	3.1(10) ^d	5.1(9) ^d	5.0(11)	3.9(10)	–	–
R/DC \rightarrow 937	[26.25]	36.5(5)	41(5)	37(2)	34.4(17)	36.8(16)	41.4(19)	[41.2(34)]
R/DC \rightarrow 1042	[1.2]	–	3.1(13)	–	0.7(4)	0.6(3)	0.2(1)	–
R/DC \rightarrow 1121	[11.1]	7(3)	5(3)	9.6(14)	10.6(12)	6.4(9)	9.2(11)	[7.7(26)]
R/DC \rightarrow 1701	[0.2]	2.2(16)	–	–	0.6(3)	–	–	–
R/DC \rightarrow 2101	[0.05]	3.3(19)	–	–	–	–	0.8(4)	–
R/DC \rightarrow 2523	[1.6]	–	2.3(15)	3.5(6)	2.5(5)	3.9(5)	3.1(4)	[4.6(13)]
R/DC \rightarrow 3062	[10.2]	9(3)	10(3)	9.9(13)	6.6(10)	6.9(9)	5.6(9)	[9.3(16)]
R/DC \rightarrow 3134	[0.04]	–	–	–	0.5(3)	–	0.8(3)	–
R/DC \rightarrow 3358	[1.2]	–	–	–	1.3(5)	0.8(5)	0.7(4)	–
R/DC \rightarrow 3724	[0.06]	3.0(14)	–	–	–	0.8(3)	0.9(2)	–
R/DC \rightarrow 3791	[1.2]	–	–	–	3.0(5)	3.9(4)	3.7(6)	[4.2(23)]
R/DC \rightarrow 3839	[19.0]	24(4)	22(3)	18.8(14)	16.9(11)	18.7(10)	19.9(10)	[17.2(17)]
R/DC \rightarrow 4116	[11.6]	12(3)	10(2)	9.1(10)	8.8(7)	8.2(6)	9.0(7)	[10.3(13)]
R/DC \rightarrow 4226	[0.1]	–	–	1.0(6)	0.8(4)	0.6(3)	–	–
R/DC \rightarrow 4398	[0.2]	–	–	–	1.5(4)	1.1(3)	1.5(4)	–
R/DC \rightarrow 4652	[4.0]	–	3.5(15)	–	1.1(4)	2.8(4)	1.7(3)	[2.4(14)]
R/DC \rightarrow 4964	[7.8]	3.0(16)	–	6.0(8)	5.7(6)	4.6(5)	1.5(5)	[3.1(12)]
E_{eff}^{cm} (keV) ^f	[165]	160.1(10)	174.5(15)	228.1(19)	255.1(13)	276.4(19)	300.7(16)	[301]
$S_{tot}(E)$ (keVb):	[4.7]	5.2(6)	4.9(6)	6.0(5)	6.1(5)	6.7(5)	6.9(5)	[7.8(5)]

^a Primary transitions to final ^{18}F states. Energies are in units of keV. The label “R/DC” refers to the sum of broad resonance tails and direct capture.

^b Based on the analysis of coincidence data, except were noted otherwise.

^c Calculated values for comparison; obtained by using resonant properties of higher-lying resonances [22], and direct capture model calculations scaled by experimental spectroscopic factors [12, 22, 45].

^d From analysis of singles data (see text).

^e Derived from Tab. I of Di Leva et al. [25], who used a single HPGe detector.

^f Effective energy in the center-of-mass system.